Arch. Metall. Mater. **64** (2019), 1, 33-38

DOI: 10.24425/amm.2019.126215

A. TELLIER*#, M.R. ARDIGO-BESNARD*, J.-P. CHATEAU-CORNU*

INFLUENCE OF THE PROCESS PARAMETERS ON THE MICROSTRUCTURE OF A HARDFACING COATING ELABORATED BY HOT ISOSTATIC PRESSING

Hot Isostatic Pressing elaboration of Norem02, an austenitic-ferritic hypereutectoid stainless steel, leads to the formation of an austenitic matrix with a mixture of acicular M_7C_3 and globular $M_{23}C_6$ carbides. The sintering tests, carried out by using an AISI 304L container, showed that the final microstructure and the carbides' distribution of the HIPed Norem02 are strongly influenced by the process parameters (heating and cooling rate, sintering time, holding temperature and pressure) and by the particles' size, microstructure and phase distribution of the initial powder. The morphological, crystallographic and chemical analysis of the sintered samples were completed by comprehension of the diffusion phenomena at the Norem02/304L interface, enabling the establishment of a correlation between elaboration process and final microstructure.

Keywords: powder metallurgy, hot isostatic pressing, high carbon steel, microstructure, hardfacing coating

1. Introduction

The shutters of the globe valves used in the primary coolant circuits of PWR nuclear power plants have to exhibit resistance against high closing pressures (103 MPa) and temperatures (633 K maximum). For these reasons, a hardfacing coating with good mechanical, wear and corrosion properties is required to protect the valve seat and lid. Several cobalt-free alloys were developed and tested to replace Stellites™. Norem™, iron-based alloys (25 wt % Cr, 4 wt % Ni, 4 wt % Mn, 3 wt % Si, 2 wt % Mo, 1.2 wt % C for Norem02), seem to be the best candidates to replace Stellites™, former alloys used as hardcoatings, which were responsible for high gamma-ray emissivity [1,2], as they present similar corrosion and mechanical properties, and good galling resistance. PTAW (Plasma Transferred Arc Welding) technique is generally used to deposit Norem02 coatings, leading to a complex and heterogeneous microstructure with insufficient tribological properties [3,4].

It is well known that the microstructure is one of the major parameters controlling the tribological response of materials [5]. Generally, a fine microstructure with strain hardening capability and small carbides, homogeneously distributed in the matrix, leads to high resistance against galling wear [5,6] The Hot Isostatic Pressing (HIP) process represents a very attractive sintering technique to obtain dense materials, with a fine-grained microstructure and better durability properties [7] and could represent an attractive alternative to the conventional coating techniques.

In the present study, the Norem02 coating deposition was elaborated by HIP using two sintering conditions with different process parameters and by using two powders with similar chemical compositions but different particles' size and morphology. In the first part, we focus on the microstructure, chemical composition and phase distribution of the initial powders and sintered samples. Then, the diffusion phenomena at the Noem02/304L container interface were investigated. The aim of these studies was to evaluate the influence of the initial powder and process parameters on the final microstructure of the sintered samples.

2. Experimental procedure

Compositions of the Norem02 powders used for the sintering tests are given in Table 1. Powder 1 was supplied by Höganäs and powder 2 by Ducal. Both powders were obtained by atomisation process.

TABLE 1

Powder 1 and powder 2 chemical compositions

Element (wt%)	Powder 1	Powder 2
Cr	24.2	24.8
Mo	2.1	2.2
Ni	3.8	4.2
Si	3.1	3.3
Mn	4.1	4.1
C	1.14	1.30
O	0.025	0.027

* LABORATOIRE INTERDISCIPLINAIRE CARNOT DE BOURGOGNE (ICB), UMR 6303 CNRS – UNIVERSITÉ DE BOURGOGNE-FRANCHE-COMTÉ, BP 47870, 21078 DIJON CEDEX, FRANCE

Corresponding author: arnold.tellier@u-bourgogne.fr

The particles' size, measured by laser granulometry, ranges from about 50 up to 150 µm for powder 1 and from 20 up to 50 µm for powder 2. HIP experiments were carried out by using a Quintus QIH-15L apparatus. The process parameters used for the sintering tests are listed in Table 2. Powders 1 and 2 were HIPed by using the parameters of Test 1 and Test 2 respectively.

TABLE 2

Parameters used for the sintering tests

Parameters	Test 1	Test 2
T°(K)	1473	1373
Pressure (Bar)	1020	1200
Holding time (h)	3	3
Heating rate ($K \cdot min^{-1}$)	10	6
Cooling rate	Natural	Natural
Container	304L	304L

The bulk densities of the sintered samples were determined by Archimedes' method. Three measurements were carried out for each sample in order to obtain an average value.

The microstructures of the powders and the HIPed samples were characterized using a JEOL JSM-6400F scanning electron microscope (SEM) equipped with a field emission gun (FEG) and coupled with an energy dispersive X-ray spectrometer (EDX). Chemical phases were identified by X-ray diffraction (XRD) using a Bruker D8-A25 diffractometer with Cu Kα radiation (λ = 0.154056 nm). To complete the microstructural investigations, optical microscope (OM) observations were carried out after Murakami etching (10 g NaOH + 10 g $K_3Fe(CN)_6$ + 100 ml H_2O, t = 45-60 s).

3. Results and discussion

3.1. Powders' characterisations

Fig. 1 (a) and (b) show SEM micrographs of the two Norem02 powders. Secondary electron images reveal that, for both powders, particles are almost spherical. SEM observations confirm that the particles' size is in good agreement with laser granulometry measurements, which showed a tighter distribution for powder 2. Particle size and distribution has a great influence on shrinkage capacity. Generally, a large particle distribution has a beneficial effect on powder sintering, as small particles fill the spaces between large ones [8].

XRD analyses (Fig. 2) confirmed the presence, for both powders, of austenite as major phase, a small amount of ferrite and a C-enriched phase with a cubic primitive structure. The latter is a metastable phase that transforms into $M_{23}C_6$ carbides, as verified by XRD diffraction after annealing at 1273 K for 10 minutes.

OM observations of the particles of the two powders were performed after chemical etching with Murakami solution, generally used to reveal $M_{23}C_6$ carbides (where M = Cr, Fe, Mo, Mn…)

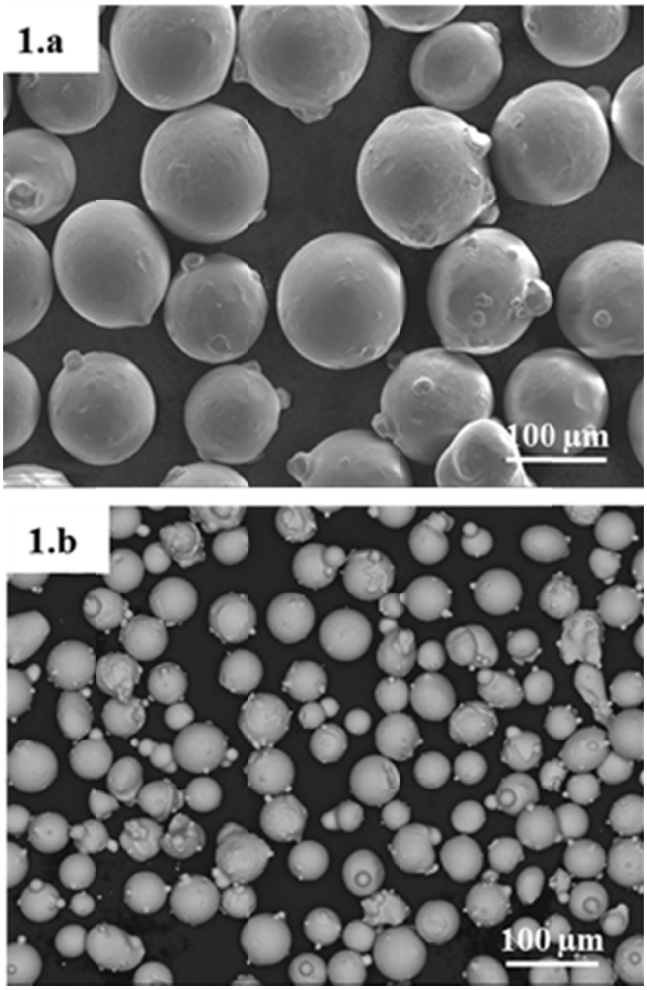

Fig. 1. SEM observations of (a) powder 1 and (b) powder 2

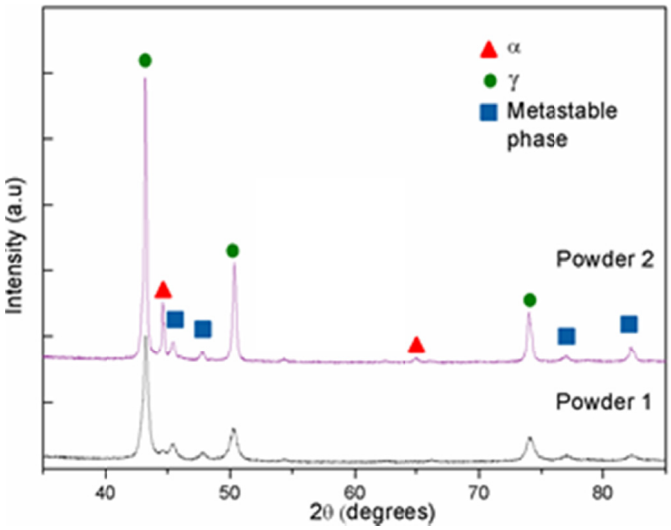

Fig. 2. XRD patterns of Norem02 powders before sintering

and ferrite (Fig. 3 (a) and (b)). The rapid solidification of liquid droplets during the atomisation process leads to the formation of austenitic dendrites, which appear in white in the OM images. The interdendritic black regions are composed of ferrite and the metastable C-enriched phase.

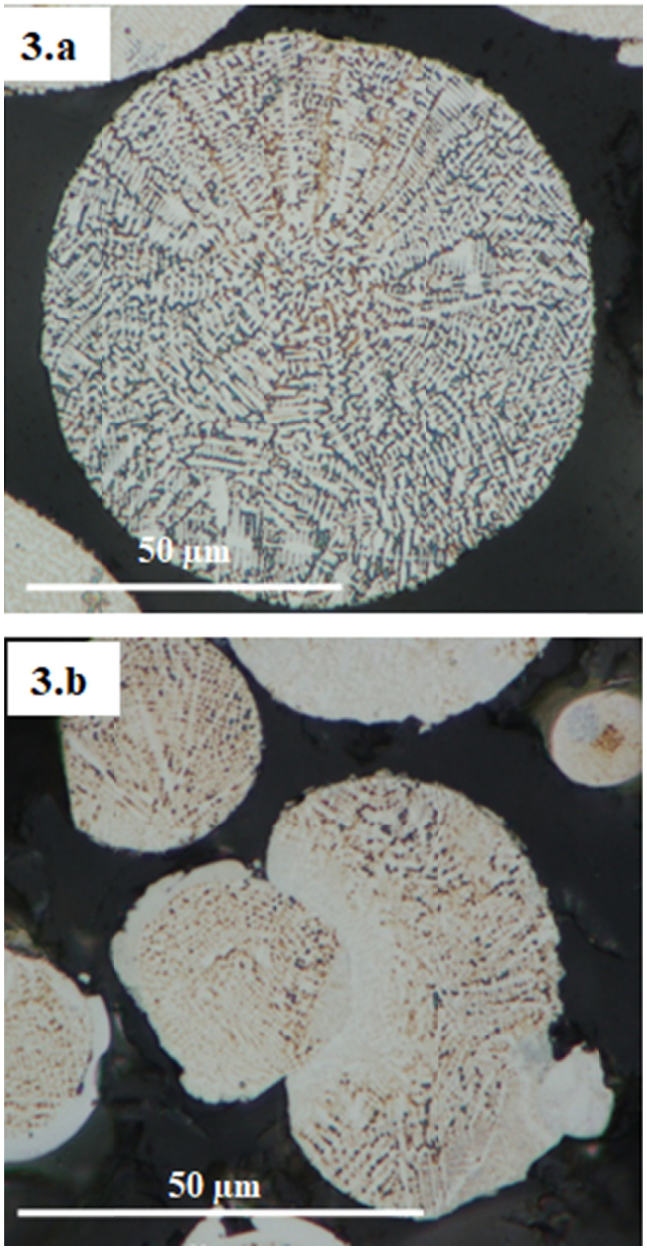

Fig. 3. OM observations of (a) powder 1 and (b) powder 2 after Murakami etching

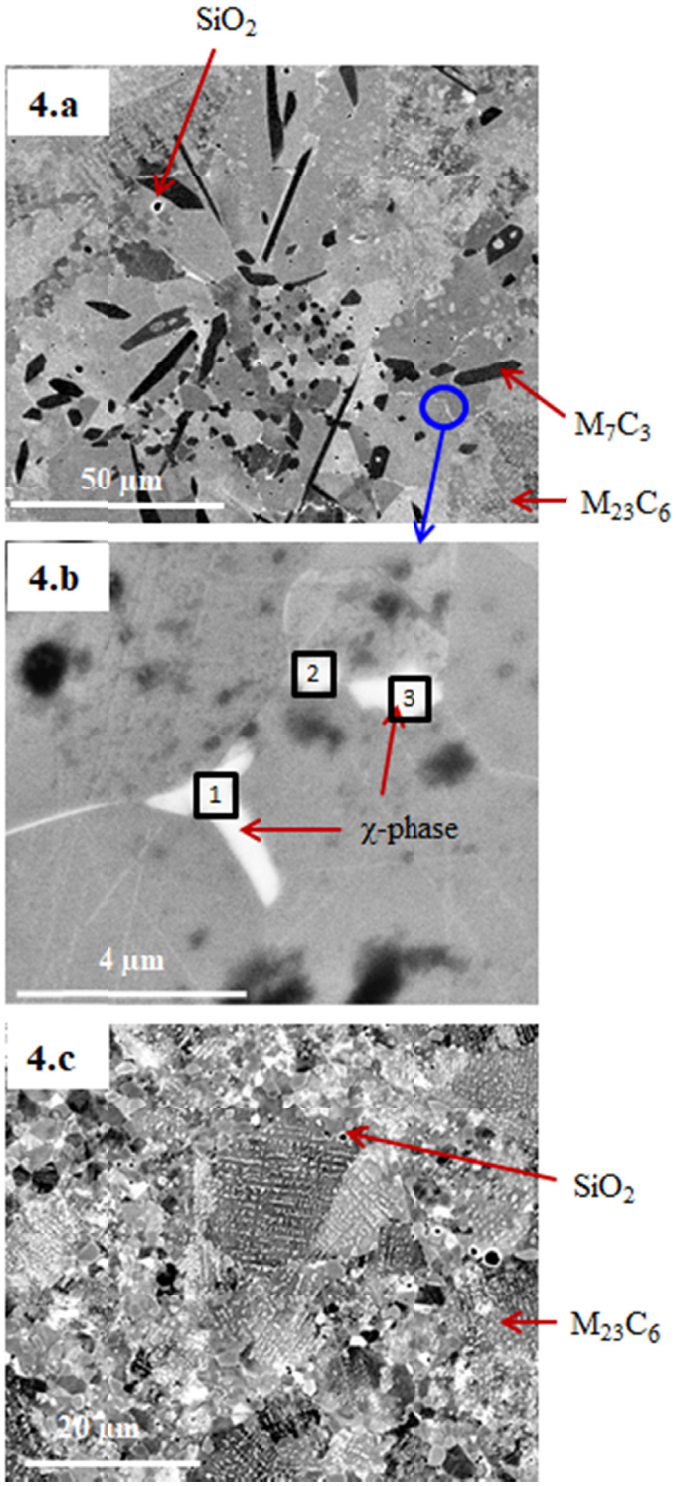

Fig. 4. SEM images of the bulk of (a) the HIPed powder 1, (b) the Mo-Si enriched phases and (c) the HIPed powder 2

3.2. HIPped samples' characterisations

3.2.1. SEM-EDX and XRD analyses of Norem02 bulk

Powder 1 which was HIPed at a lower pressure has not been fully compacted (98.9%) contrary to powder 2. SEM micrographs of the bulks of the sintered samples are shown in Fig. 4.

SEM-EDX and XRD analyses of the bulk of the HIPed powder 1 (Fig 5) reveal the presence of austenite as major phase and of a very small amount of ferrite. Big acicular M_7C_3 carbides (where M is mainly Cr and Fe as confirmed by EDX analyses) and globular $M_{23}C_6$ carbides (where M is mainly Cr, Mo and Mn) are randomly distributed in the austenitic matrix.

Mo-Si enriched phases were detected mainly at grain boundaries and close to M_7C_3 carbides (Fig. 4 (b)). The amount of Mo detected by EDX (Table 3) suggests the presence of χ-phases, as described by several authors [9-12]. However, it should be noticed that χ-phase stoichiometry depends strictly on the alloy composition and it is not possible to assign it an exact formula based on the available literature data. For this reason, further characterisations are needed and will be performed in order to better investigate the nature of the Mo-Si enriched phases and their formation.

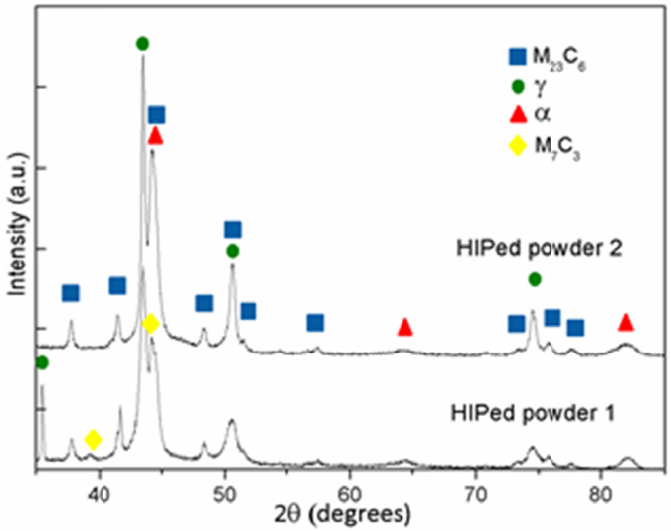

Fig. 5. XRD patterns of HIPped samples

HIPed powder 2 (Fig. 4 (c)) presents a fine microstructure, close to that observed before sintering (Fig. 3 (b)), composed of austenite, a very small amount of ferrite and small-sized $M_{23}C_6$ carbides, as indicated by EDX measurements coupled with XRD analyses (Fig. 5). A Mo-Si enriched phase was not detected at grain boundaries or close to the carbides.

TABLE 3

Chemical composition of Mo-Si enriched phase (wt %)

Zone	Si	Cr	Mn	Fe	Ni	Mo
1	6.4	22.3	5	53.1	4.7	8.5
2	6.1	22.5	5.2	52.9	4.7	8.6
3	6.1	22.1	5.2	54	4.8	7.9

For both HIPed samples some inclusions, mainly Si-enriched oxides, were detected by EDX analyses and appear in black in SEM images (Fig. 4 (a) and (c)).

Based on the pseudo-binary phase diagram of the Fe-Cr-Mo-C system containing Fe – 25 wt% Cr – 5 wt% Mo calculated by Wieczerzak et al. [13], it is possible to suggest that the formation of M_7C_3 carbides for the HIPed powder 1 is due to the sintering temperature. Indeed, for a carbon content of 1.14 wt% and a temperature of 1473 K (case of powder 1), the pseudo-binary diagram indicates the presence of a mixture of M_7C_3 and $M_{23}C_6$ carbides. On the other hand, for a carbon content of 1.3 wt% and a temperature of 1373 K (case of powder 2), the M_7C_3 carbides' precipitation is not possible.

EDX measurements performed on both samples showed the formation of a chromium depleted zone (CDZ [14]) about 10 µm wide around the M_7C_3 carbides, while CDZs below 1 µm in width are observed around the $M_{23}C_6$ carbides in SEM. In this area, the chromium amount decreases to nearly 18-19 wt%, while it is around 24 wt% in the austenitic matrix. Chromium carbides are known to improve mechanical properties as tensile strength, hardness and wear resistance [15]. However, CDZs resulting from carbides and/or χ/σ-phase precipitation can affect the alloy electrochemical corrosion resistance, as reported by some authors [16-19].

3.2.2. SEM-EDX analyses of Norem02/304L interface

SEM images of the Norem02/304L interface are shown in Fig. 6. For the HIPed powder 1 (Fig. 6 (a)), some Mo-Si enriched phases, appearing in white colour in SEM micrographs, were detected on grain boundaries inside the Norem02, close to the interface with the container. As previously discussed, comparison with literature data suggests they are χ-type phases. Close to the interface, the acicular M_7C_3 carbides are not present in the Norem02 and only globular $M_{23}C_6$ carbides, having a bigger size than those observed in the bulk, are detected and are visible in the EDX carbon and chromium mappings.

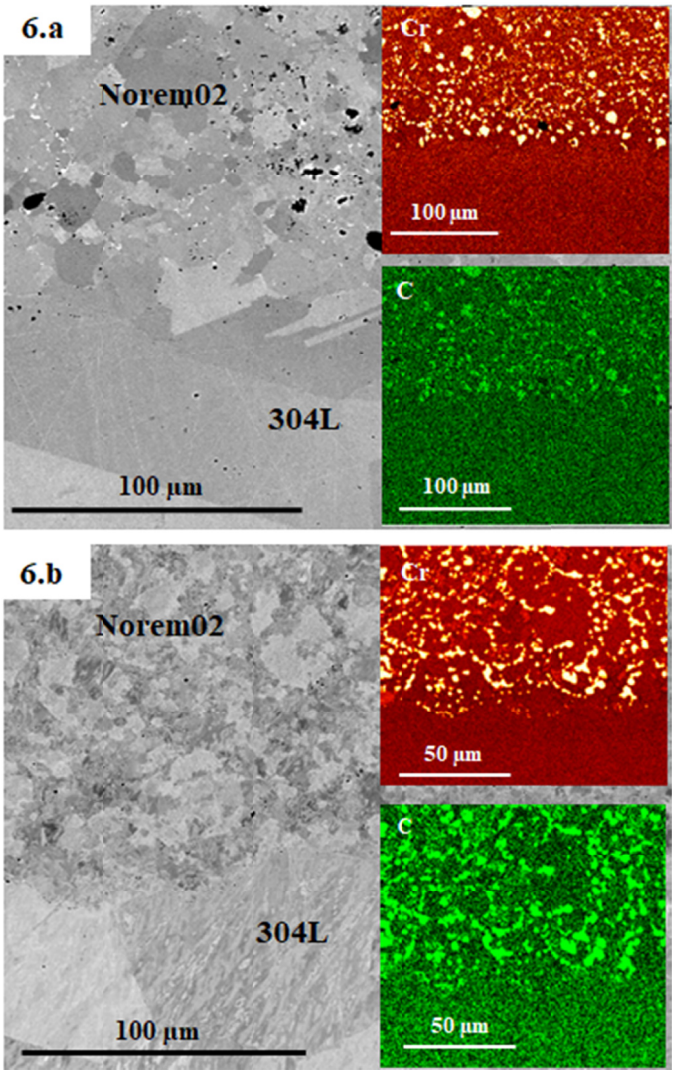

Fig. 6. SEM images of Norem02/304L interfaces with C and Cr mapping: (a) HIPed powder 1 and (b) HIPed powder 2

In the case of the HIPed powder 2 (Fig. 6 (b)), no Mo and Si-enriched intergranular phase was revealed by SEM-EDX close to the Norem02/304L interface. Moreover, in this region, $M_{23}C_6$ carbides coalesced, as observed for HIPed powder 1 and illustrated by SEM mappings of elements.

For the two HIPed samples interfaces, a depletion of nickel inside the 304L container was detected by EDX and is illustrated by the nickel SEM mapping (Fig. 7). Close to the interface with Norem02, the amount of nickel decreases to 4 wt% inside the 304L steel; EDX analyses revealed that at only 30 µm depth inside the 304L container, nickel reaches its nominal value of 9 wt%. On the other hand, EDX measurements did not show any accumulation or depletion of nickel inside Norem02. Further characterisations are planned in order to better investigate this phenomenon.

4. Conclusions

Two Norem02 powders, having a similar chemical composition but different granulometries and microstructures, were HIPed with different process parameters: 1473K-1020 bar and 1373K-1200 bar. The first one was incompletely compacted and M_7C_3 and $M_{23}C_6$ carbides formed in the austenitic matrix. Moreover, Mo and Si enriched phases (probably χ-phases) were detected at grain boundaries. The second one was completely compacted. Only $M_{23}C_6$ carbides were detected in the austenitic matrix and a Mo and Si enriched phase did not form at grain boundaries. By comparison with the thermodynamic simulations available in literature, the formation of M_7C_3 carbides for powder 1 can probably be explained by the sintering temperature. On the other hand, the difference in bulk density between the two HIPed powders is influenced by pressure and/or powder compressibility. The powder with the tightest particle size distribution exhibited a higher final density, which contradicts what is generally reported in the literature. Further investigations are planned in order to better understand the parameters influencing the powder compaction.

At the Norem02/304L container interfaces, only $M_{23}C_6$ carbides were revealed inside the Norem02 for the two HIPed samples. These $M_{23}C_6$ carbides have a larger size than those observed in the bulk. A nickel depletion zone was revealed in the 304L steel at the interface with Norem02, but no nickel depletion or accumulation was observed in Norem02, the understanding of which requires further investigations. Only for the HIPed powder 1, Mo and Si-enriched phases were detected at Norem02 grain boundaries close to the interface with the 304L steel.

Acknowledgments

The authors would like to thank the Bourgogne-Franche-Comté Region for financing part of this study and FRAMATOME which finances the Chair in which this program is included.

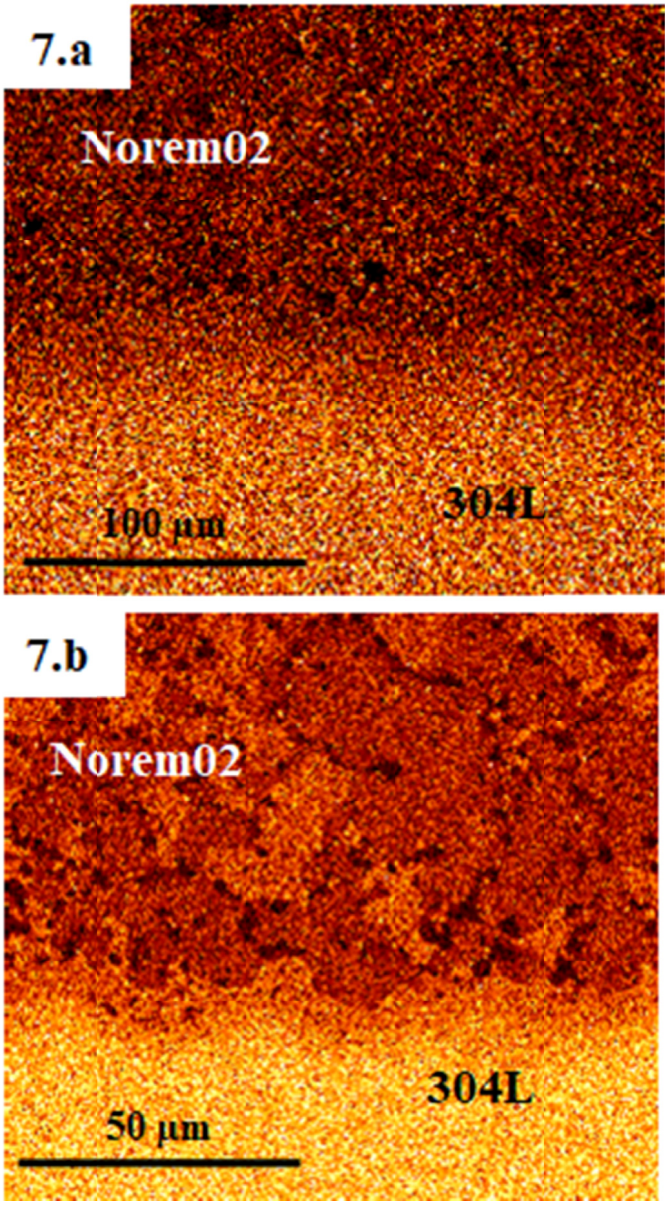

Fig. 7. SEM nickel mappings of Norem02/304L interfaces: (a) HIPed powder 1 and (b) HIPed powder 2

REFERENCES

[1] H. Ocken, Surf. Coat. Technol. **76**, 456-461 (1995).
[2] Ek. Ohriner, T. Wada, E. P. Whelan, H. Ocken, Metall. Trans. **22** (5), 983-991 (1991).
[3] G. Beaurin, J.-P. Mathieu, E. Gauthier, D. Nelias, M. Coret, F. Arnoldi, Mater. Sci. Eng. A. **528** (15), 5096-5105 (2011).
[4] D.H. Persson, S. Jacobson, S. Hogmark, Wear **255** (1-6), 498-503 (2003).
[5] G.A. Fontalvo, R. Humer, C. Mitterer, K. Sammt, I. Schemmel, Wear **260** (9-10), 1028-1034 (2006).
[6] A. Dalmau, C. Richard, A. Igual – Muñoz, Tribol. Int. **121**, 167-179 (2018).
[7] V. Viswanathan, T. Laha, K. Balani, A. Agarwal, S. Seal, Mater. Sci. Eng. R Rep. **54** (5-6), 121-285 (2006).

[8] H.V. Atkinson, S. Davies, Metallurgical and Materials Transactions A. **31** (12), 2981-3000 (2000).

[9] D.M. Escriba, E. Materna-Morris, R.L. Plaut, A.F. Padilha, Mater. Charact. **60** (11), 1214-1219 (2009).

[10] J. Michalska, M. Sozańska, Mater. Charact. **56** (4-5), 355-362 (2006).

[11] I. Calliari, M. Zanesco, E. Ramous, J. Mater. Sci. **41** (22), 7643-7649 (2006).

[12] N. Llorca-Isern, H. López-Luque, I. López-Jiménez, M.V. Biezma, Mater. Charact. **112**, 20-29 (2016).

[13] K. Wieczerzak, P. Bala, M. Stepien, G. Cios, T. Koziel, Mater. Des. **94**, 61-68 (2016).

[14] K. Wieczerzak, A. Żywczak, J. Kanak, P. Bała, Mater. Charact. **132**, 293-302 (2017).

[15] C. García de Andrés, G. Caruana, L. Alvarez, Mater. Sci. Eng. A. **241** (1-2), 211-215 (1998).

[16] E.L. Hall, C.L. Briant, Metall. Trans. A. **15** (5), 793-811 (1984).

[17] T. Thorvaldsson, G.L. Dunlop, J. Mater. Sci. **18** (3), 793-803 (1983).

[18] P. de Lima-Neto, J.P. Farias, L.F.G. Herculano, H.C. de Miranda, W.S. Araújo, J.-B. Jorcin, N.e Pébère, Corros. Sci. **50** (4), 1149-1155 (2008).

[19] T. Takei, M. Yabe, F.-G. Wei, Corros. Sci. **122**, 80-89 (2017).